Performance of density-functional-theory and random-phase-approximation methods on the study of transition-metal clusters: the Ta_n clusters as an example

Jesús R. Flores[a], Detlef Schooss[b] and Wim Klopper[b,c]

[a]Departamento de Química Física, Facultade de Química, Universidade de Vigo, Vigo, Spain; [b]Institute of Nanotechnology, Karlsruhe Institute of Technology, Karlsruhe, Germany; [c]Institute of Physical Chemistry, Karlsruhe Institute of Technology, Karlsruhe, Germany

ABSTRACT

Recently developed density-functional-theory (DFT) and random-phase-approximation (RPA) methods are used to study competing isomers of some negatively charged Ta clusters, namely Ta_{12}^- and Ta_{10}^-, in an attempt to find a suitable strategy towards accurate studies of transition-metal clusters based on DFT. Also the neutral and cationic forms $Ta_{12}^{(0,+)}$ of the twelve-atom cluster are studied. The results are compared with experimental information obtained by several methods that differ in the property under study and the total electric charge of the clusters. We find that a careful choice of the density functional, the use of relativistic two-component methods, eventually in combination with all-electron basis sets, and the application of RPA-type methods, may all be necessary steps for a good assessment. Such an assessment should be made in relation to several experimental properties as much as possible.

KEYWORDS

Density-functional methods; random-phase-approximation methods; metal clusters

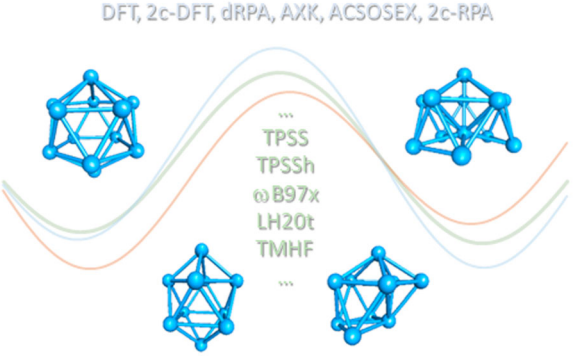

1. Introduction

The structures of negatively charged Ta clusters, Ta_n^-, $6 \le n \le 13$, were recently studied by combining the trapped-ion electron-diffraction method (TIED) with several electronic-structure methods [1]. In most cases, the electronic-structure methods predicted the structurally best fitting isomer to be the energetically lowest lying one, so there was agreement between theory and experiment in that respect. In the case of Ta_{12}^-, however, the electronic-structure methods disagreed with experiment, to some extent also in the case of Ta_{10}^-. Such a situation is not unusual in studies of metal clusters, which is most frequently done by density-functional-theory (DFT) based methods, since different functionals, basis sets, and pseudopotentials may energetically favour different motifs.

In the case of Ta_{12}^-, the computational methods employed seemed to point to an icosahedral cage as the most stable structure, while a four-atom-capped hexagonal bi-pyramid and several geometrically close-lying isomers based on the pentagonal bi-pyramid motif were found to display higher energies by most of the methods employed, even the most advanced ones. Those methods included several density functionals, the

CONTACT Jesús R. Flores flores@uvigo.es Departamento de Química Física, Facultade de Química, Universidade de Vigo, 36310 Vigo, Pontevedra, Spain

direct random-phase approximation (dRPA), and two-component (2c) DFT computations, including spin–orbit coupling. In principle, there are two possible explanations to such a discrepancy, which are not incompatible. First, the formation of the icosahedral cage isomer could be prevented by large energy barriers, even if it were the most stable one. Second, that isomer could, in reality, be not the most stable: one would need a very precise selection of the electronic structure methods in order to determine the right energy ordering.

Quite recently, there have been key advances in the development of DFT [2,3], RPA-type [4–10], and relativistic two-component (2c) methods [11,12], which could help devise a better approach to the study of, for instance, metal clusters, and perhaps, solve some of the existing discrepancies between theory and experiment.

Some local-hybrid density functionals have been developed [2,13–16], also range-separated [17,18] and long-range-corrected [19] functionals, which provide very good performance in a number of tests, normally superior to that of the generalised gradient approximation (GGA) or meta-GGA (MGGA) functionals, even if exact exchange is added to the latter. There is little experience on the performance of all those functionals in combination with 2c methods, specifically not for metal clusters. Moreover, there are relatively recent developments in RPA-type methods, by adding perturbative corrections, such as the second-order exchange (SOX), second-order screened exchange (SOSEX) and approximate-exchange-kernel (AXK) methods [5,6]. There are also some developments in 2c-RPA theory [8,9] (Kramers-restricted), including, very recently, a non-restricted version [10].

Applying all those kinds of theoretical methods together could be interesting, in part because the experimental information on metal clusters comes from different sources [20,21]. One may have for instance, quite precise information on the cluster geometries by TIED experiments [22–24], on the vibrational spectrum [20], and on the magnetic moments or dipole moments (or polarizabilities) by magnetic or electric deflection experiments [25–28] or X-ray magnetic circular dichroism (XMCD) [29]. In all those experiments the clusters might have different total charges, and different cluster-generation procedures could have been used too. Therefore, one might need to use a combination of theoretical methods in order to fully understand the body of experimental information.

In the present case, apart from the TIED experiments already mentioned [1], we have the infrared-multiphoton-dissociation (IR-MPD) experiments by Fielicke's group on the Ta_{6-20}^{+} series [30], the electric-deflection experiments by Moro *et al.* [25], and the magnetic-deflection experiments by Diaz-Bachs *et al.* [31]. There are also some reactivity studies, the first by Hamrick *et al.* [32], who suggest the existence of two isomers of Ta_{12}. The threshold ionisation potentials of Ta_{3-64} have been obtained by Collings *et al.* using photoionization-efficiency spectra [33]. There are also time-of-flight mass spectrometry (TOFMS) [34] and Coulomb-explosion experiments carried out by strong-field ionisation of Ta_n clusters ($n < 30$) [35]. Ta_3 has been the subject of a Raman-spectroscopy study in an Ar matrix [36] while Ta_3^- has been investigated by photoelectron spectroscopy and DFT computations [37]. It must be noted, as pointed out in those experimental studies, that Ta, either in cluster or nanoparticle form, is quite interesting from the chemical point of view [38–47].

There are many theoretical studies on $Ta_n^{(+,0,-)}$ clusters of different sizes, most of them by DFT, using GGA or MGGA functionals, sometimes incorporating exact exchange in a global-hybrid form [1,48–55]. These studies include the structures of neutral clusters $n \leq 78$, studied by molecular dynamics using an analytical potential by Jiang *et al.* [48], also using DFT, by Kraft *et al.* [1] for $6 < n < 13$ with a genetic algorithm [GA], for $2 < n < 17$ by Li *et al.* [52], for $n = 2$–23 by Fa *et al.* [49], and more recently by Han *et al.* [55] for $n = 9$–13. Du *et al.* [53] have studied cationic clusters $6 < n < 16$ by DFT and compared their simulated IR spectra with the experimental spectra of Gruene *et al.* [30]. More recently, Huang *et al.* [56] have conducted a wide study on the reactions of Ta_n^- with N_2 up to $n = 57$, using a TOFMS, combined with photoelectron spectroscopy (PES) for Ta_{10}^-, which reveals the appearance of the bi-capped square antiprism isomer in that experiment.

The purpose of the present work is to clarify the disagreement between theory and experiment in the case of Ta_{12}^-, also in Ta_{10}^-, by using some of recently developed theoretical methods. We will pay some attention to $Ta_{12}^{(0,+)}$ too. Our work might help, we believe, to find a better computational strategy for the study of metal clusters.

2. Computational details

We have determined the equilibrium geometries by the TPSSh/dhf-TZVP and BH-LYP/dhf-TZVP methods for a few competing isomers of Ta_{12}^-, numbered **1** to **5**, in several electronic states. The simulated scattering functions from the equilibrium geometries are in good agreement with those from the TIED experiment for isomers **3** to **5**, especially for the latter [1]. In those geometry optimizations the MGGA hybrid functional of Tao, Perdew, Staroverov and Scuseria [57] (TPSSh) or the GGA hybrid

BH-LYP (consisting of Becke's 88 exchange plus 50% exact exchange and Lee–Yang–Parr correlation) have been used [58,59]. On the optimised geometries we have carried out DFT computations with a number of density functionals, mainly with TPSSh, BH-LYP, the long-range corrected hybrid ωB97x of Chai and Head-Gordon [19], and the recently developed TMHF density functional of Holzer and Franzke [16], using larger basis sets, namely what we call the dhf-TZVPPD-2c and dhf-QZVPPD-2c [61] basis sets, which are just the corresponding dhf-(T/Q)ZVPP-2c basis sets plus a *p* shell with exponent $0.27701105074 \cdot 10^{-1}$ (T) or $0.20413673674 \cdot 10^{-1}$ (Q). Those exponents are the same as those of the diffuse *p* shells in the def2-TZVPPD and def2-QZVPPD basis sets. We have also performed dRPA computations using the Kohn–Sham spin-orbitals obtained with a number of density functionals and basis sets, at least with dhf-TZVPPD-2c, although, following references [6,7], we attach more relevance to the dRPA results obtained with the TPSSh density functional, which are quite similar to those obtained with TPSS [60], also in the present case. In some selected cases, beyond-RPA calculations, such as second-order-screened-exchange (SOSEX) and approximate-exchange-kernel (AXK) calculations [5,6] have also been done.

In addition, we have conducted two-component DFT computations (2c-DFT), which incorporate spin–orbit coupling, using the dhf-TZVP-2c and dhf-TZVPPD-2c basis sets [61]. Selectively, we have performed 2c-RPA computations, of the direct type, on some isomers of Ta_{12}^-, as well as on the corresponding isomers of the neutral system, and also on two isomers of Ta_{10}^-.

The dhf-TZVP(-2c), dhf-TZVPPD-2c and dhf-QZVPPD-2c [61] basis sets have been used together with the dhf-ecp-2c pseudopotential [62] and the universal-ecp-60 basis [63] as auxiliary RI-J basis set. The def2-TZVPPD and def2-QZVPPD auxiliary basis sets [64] have been used for RPA-type TZ and QZ computations, respectively. It must be noted that the dhf-TZVPPD and, especially, the dhf-QZVPPD basis give dRPA results which are quite close to their relativistic counterparts, but the latter were preferred for consistency with the 2c-RPA and DFT computations.

In a few cases, we have done all-electron 2c computations by the X2C Hamiltonian [12] incorporating spin–orbit coupling, using the x2c-TZVPall-2c or x2c-TZVPPall-2c basis sets and the corresponding auxiliary RI-J basis [65].

We have also carried out a wider but straightforward study about the dependence of the energy difference between isomers **5** and **2** of Ta_{12}^- on the density functional, as it is one of the keys to a better description of Ta clusters, probably of metal clusters in general. For that purpose, a relatively large set of density functionals have been employed, from simple LDA-type like S-VWN [66–68] to the recently developed local hybrids like LH20t [15] or TMHF [16].

We have employed the multiple grid m5 for DFT and RPA-type computations, g5 for 2c-DFT and 2c-RPA, and the radially enlarged 5a [69] for the all-electron X2C computations.

All the computations have been done with either Turbomole 7.3 or Turbomole 7.7 [70].

3. Results and discussion

The structures of the Ta_{12}^- isomers studied in the present work are presented in Figure 1. Isomer **1** is four-atom-capped hexagonal bi-pyramid. Isomer **2** is an icosahedral cage structure, whereas isomers **3** to **5**, which may be considered incomplete icosahedrons, have a pentagonal bi-pyramid motif with a five-atom cap surrounding one tip, and differ mostly in how much the cap is open on one side. Therefore, isomers **3** to **5** can be seen as distorted forms of a C_{5v} structure (not shown), which happens to be a saddle point, so they are quite close geometrically and energetically. For each isomer, optimised geometries for electronic states of several spin multiplicities can normally be obtained, although in the case of isomers **3** to **5**, also depending on the density functional, some electronic states cannot be represented by a local minimum corresponding to that isomer. The optimised geometries have been obtained by the TPSSh/dhf-TZVP and BH-LYP/dhf-TZVP methods. On the latter set of geometries, BH-LYP- and ωB97x-based single-point computations have been done, while the former set has been employed for the rest of the computations, mostly using the TPSSh, TMHF, and the ωB97x density functionals.

It should be recalled that isomers **1** and **2** are far from providing a good fit to the experimental TIED data, so they can be discarded as being present in the TIED experiment [1], while isomer **5** provides a scattering profile in very good agreement with the experimental one. To a lesser extent, isomers **3** and **4** are also consistent with the TIED data. However, **1**, and especially **2**, are very competitive in energy. In fact, as we have already mentioned and will see again, the latter (isomer **2**) appears as lowest-lying isomer by most methods, often being by 1 eV or even more lower than isomers **3** to **5**.

It must also be recalled that many more isomers were considered in our previous study, which was based on the use of a genetic algorithm [1], but it was **5** that gave the best agreement with the TIED experiments, with a very low value for the profile factor.

In order to find a good strategy towards a reasonably reliable determination of the relative energies of the

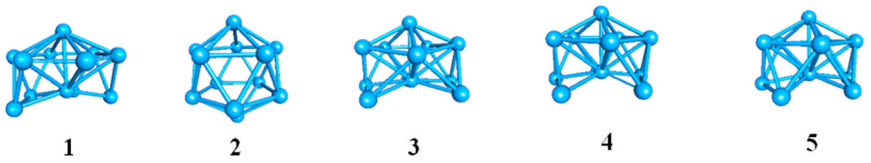

Figure 1. The Ta_{12}^- isomers considered in the present work.

Table 1. Basis-set dependence of the TPSSh and dRPA@TPSSh relative energies (given in eV) for several electronic states of isomers **1**-**5**. All computations are performed on the TPSSh/dhf-TZVP optimised geometry of the corresponding electronic state unless it is specified otherwise.

Isomer	Term/Symm	ΔE dhf-TZVP	ΔE dhf-TZVPPD-2c	ΔE dhf-QZVPPD-2c	ΔE/dRPA dhf-TZVPPD-2c	ΔE/dRPA dhf-QZVPPD-2c
1	$^2A''/C_s$	0.27	0.33	0.32	0.24	0.11
	$^4A/C_1$	0.53	0.60	0.59	0.51	0.39
2	$^4A_u/C_i$	0.00	0.00	0.00	0.07	0.03
	$^2A_2/C_{5v}$	0.06	0.09	0.08	0.00	0.00
	$^6A_g/C_i$	1.36	1.33	1.33	1.38	1.32
3	$^2A''/C_s$	0.39	0.46	0.45	0.25	0.15
	$^4A/C_1$	0.41	0.48	0.47	0.31	0.22
	$^6A/C_1$	0.55	0.62	0.66	0.59	0.52
4	$^2A/C_s$	0.50	0.58	0.57	0.26	0.15
5	$^4A/C_1$	0.54	0.60	0.58	0.42	0.31
	$^2A/C_1$ [(a)]	0.63	0.68	0.66	0.48	0.37
	$^6A/C_1$ [(a)]	0.75	0.80	0.78	0.76	0.65

(a) Using the $^4A/C_1$ TPSSh/dhf-TZVP optimised geometry.

three motifs, we first examine the sensitivity of the DFT and dRPA values to geometry and density-functional changes.

Table 1 presents the TPSSh-based energy differences calculated with several basis sets. The DFT values do not change much from dhf-TZVP to dhf-QZVPPD-2c. The dhf-TZVPPD-2c and dhf-QZVPPD-2c basis sets give almost the same values, whereas dhf-TZVP agrees within 0.1 eV. The dRPA calculations use the TPSSh Kohn–Sham orbitals and energies so they are noted as dRPA@TPSSh. The resulting relative energies are, as one would expect, more sensitive to the basis set, although still, the dhf-TZVPPD-2c values are quite close to the dhf-QZVPPD-2c ones, the difference being less than 0.13 eV. With the latter basis set one gets quite small energy differences between the three motifs, which lie within 0.15 eV, isomer **2** being the lowest lying. The dRPA@TPSSh method reduces the energy differences as compared to TPSSh, but also gives **2** as the lowest-lying isomer. By both methods, a doublet is clearly the spin multiplicity of the lowest-lying electronic state of isomer **1**, while for isomers **2** and **3** to **5**, the quartet and the doublet multiplicities are quite close, even the sextet being competitive in the case of isomers **3** to **5**.

The TPSSh and BH-LYP density functionals were found in our previous study to behave very differently so they can be taken, to some extent, as representative of two limiting cases in DFT behaviour. For that reason, we have done the same DFT computations of Table 1 with the BH-LYP density functional (see Supplemental Data, SD, Table S1). The energy differences between isomer **2** and all other isomers are higher than with TPSSh, the basis-set dependence is also weak enough, with a maximum difference of 0.12 eV. With the dhf-QZVPPD-2c basis set, the smallest energy difference between isomers **3** to **5** and **2** is found for isomer **3** at 0.87 eV using BH-LYP, whereas the same difference is 0.45 eV in the case of TPSSh, also for **3**. Note that the spin multiplicities from doublet to sextet are nearly degenerate for isomer **5**, which is closer geometrically to C_{5v} symmetry, and therefore closer to the Jahn–Teller instability locus than isomers **3** and **4**.

For the calculations with the ωB97x and TMHF density functionals, we use the TPSSh geometries, but, in the case of ωB97x, we have tested the sensitivity to geometry changes by using the BH-LYP optimised geometries as well. It must be noted that the TPSSh and BH-LYP optimised geometries are, in the case of isomers **3** to **5**, significantly different. Also, that ωB97x gives energy differences which are closer to the BH-LYP than to the TPSSh values. In Table S2 of the SD, it can readily be seen that the **1**−**2** energy differences are not very dependent on the geometry optimisation level, while the (**3**,**4**,**5**)−**2** ones differ a little bit more, but still, the minimum values are very close, 0.83 eV (TPSSh geometry of **5**) and 0.84 eV (BH-LYP geometry of **3**).

Table 2 summarises the DFT energy differences obtained with the four density functionals in combination with several basis sets. It is readily seen that BH-LYP and ωB97x present structure **2** as the lowest-lying by about 0.9 eV while TPSSh and TMHF give much smaller

Table 2. Summary of the DFT energy differences for isomers **1**–**5** calculated with the TPSSh, BH-LYP, ωB97x, and TMHF density functionals in the corresponding lowest-lying multiplicity for each isomer and density functional.

	ΔE/eV				
Isomer	1	2	3	4	5
TPSSh					
dhf-TZVP	0.27	0.00	0.39	0.50	0.54
dhf-TZVPPD-2c	0.33	0.00	0.46	0.58	0.60
dhf-QZVPPD-2c	0.32	0.00	0.45	0.57	0.58
BH-LYP					
dhf-TZVP	0.83	0.00	0.78	1.00	1.12
dhf-TZVPPD-2c	0.93	0.00	0.90	1.08	1.21
dhf-QZVPPD-2c	0.95	0.00	0.87	1.10	1.22
ωB97x					
dhf-TZVP	1.32	0.00	1.01	1.22	0.85
dhf-TZVPPD-2c	1.35	0.00	1.02	1.21	0.83
TMHF					
dhf-TZVP	0.63	0.00	0.47	0.60	0.21
dhf-TZVPPD-2c	0.66	0.00	0.49	0.62	0.21

Table 3. 2c and X2C DFT comparison of the **5**−**2** energy difference. N_s represents the average number of unpaired electrons. The basis sets dhf-TZVP-2c, dhf-TZVPPD-2c, and the all-electron basis x2c-TZVPall-2c have been used. $\Delta E(\mathbf{5}-\mathbf{2}) \equiv E(\mathbf{5}) - E(\mathbf{2})$.

Density functional	Basis	$\Delta E(\mathbf{5}-\mathbf{2})$/eV	$N_s(\mathbf{5})$	$N_s(\mathbf{2})$
TMHF[a]	dhf-TZVP-2c	0.14	4.12	1.92
TMHF[a]	dhf-TZVPPD-2c	0.12	4.04	1.97
TMHF[a],[c]	x2c-TZVPall-2c	−0.18	3.49	1.89
TMHF[b]	dhf-TZVP-2c	0.33	3.92	1.75
TPSSh[a]	dhf-TZVP-2c	0.59	2.76	2.07
TPSSh[a]	dhf-TZVPPD-2c	0.62	2.76	2.07
TPSSh[a],[c]	x2c-TZVPall-2c	0.34	2.46	2.06
BH-LYP[b]	dhf-TZVP-2c	1.19	2.26	1.61
BH-LYP[b],[c]	x2c-TZVPall-2c	0.88	1.68	1.57
ωB97x[a]	dhf-TZVP-2c	0.69	3.67	1.63
ωB97x[b]	dhf-TZVP-2c	0.88	3.95	1.34

(a) Using the TPSSh/dhf-TZVP geometries for the quartet states, ^4A_u (isomer **2**) and ^4A (isomer **5**).
(b) Using the TPSSh/def2-SVP geometries for the quartet states, ^4A_u (**2**) and ^4A(**5**).
(c) Exact two-component approach [12].

energy differences. Interestingly, TMHF favours isomer **5**, the best TIED-fitting one, as the second most stable, while, in contrast to TPSSh, the **1**−**2** difference is quite large. Thus, TMHF seems to agree much closer with the TIED experiments than even TPSSh. In general, TPSSh and TMHF on the one hand, and BH-LYP and ωB97x on the other, behave very differently from the other couple. The dhf-TZVPPD-2c and dhf-QZVPPD-2c basis sets give very similar values.

We have further done 2c-DFT computations with the dhf-TZVP-2c and dhf-TZVPPD-2c basis sets as well as all-electron computations using the exact X2C Hamiltonian on the **5**−**2** energy difference. The results are given in Table 3.

In all those computations, spin–orbit coupling is included self-consistently. The results are substantially different from all of the former computations. With the TMHF functional, one obtains energy differences of small magnitude: 0.12 eV with the dhf-TZVPPD-2c basis set and, remarkably, −0.18 eV by the X2C method with the x2c-TZVP-all-2c basis set, the latter being the only computation so far which predicts isomer **5** to be lower than **2**. With the TPSSh and the BH-LYP functionals there is a similar reduction in the **5**−**2** relative energy from dhf-TZVPPD-2c to x2c-TZVPall-2c, but the X2C energy difference is still positive, although relatively small for TPSSh.

Considering Tables 1–3, it is clear that the choice of the density functional is probably the most important factor determining the energy difference between motifs, more than the effect of the optimised geometry, the spin multiplicity, or even the type of electronic-structure method employed.

Therefore, we have tested a number of density functionals of different types: LDA, GGA and MGGA including global hybrids, as well as local and range-separated hybrids. We have done the computations on isomers **2**, **5**, and also on a C_{5v} structure, a saddle point noted as $\mathbf{sC_{5v}}$, geometrically very close to **5**, which can be seen as a Jahn–Teller distortion from the $\mathbf{sC_{5v}}$ structure. We have employed the TPSSh/dhf-TZVP optimised geometries. Although the optimised geometry would not vary much with the density functional in the case of isomer **2**, there are significant variations in the case of isomer **5**, so we use the $\mathbf{sC_{5v}}$ structure as a second reference, which could be more consistent along the density functional list. The $\mathbf{sC_{5v}}$−**5** energy differences are very small in most cases but note that they do not have to be positive, except for TPSSh. The most relevant results are presented in Figure 2, which are the values obtained with the S-VWN [66,67,68], PWLDA [66,67,71], BP86 [66,67,68,72,73], B-LYP [59,66,67,72], B-VWN [66,67,68,72], PBE [66,67,71,74], B97 [75], B97-1 [76], TPSS [60], BH-LYP [58,59,66,67,72], B3-LYP [59,66,67,68,72,77], PBE0 [66,67,71,74,78], VSXC[79], M06 [80], TPSSh [57,60,66,67,71], LH07t-SVWN [66,67,68,81], LH12ct-SsifPW92 [66,67,71,82], LH14t-calPBE [66,67,71,74,83,84], CAM-B3LYP [59,77,85], LH14 [14,72], ωB97x [19,75], HSE06 [17,74,78], LRC-ωPBEh [74,86], MPSTS [13,60], LH20t [15,74,87] and TMHF [16,88] functionals. More information is given in Figures S1 to S3 of the SD. The m5 grid has been used in all these tests and found to be sufficient for all kinds of functionals by numerical sensitivity tests.

It is immediately seen that very few density functionals give a small or negative **5**−**2** energy difference. Among those are TMHF, LH20t, TPSS, and TPSSh. Comparing the values given by some global hybrids with their GGA or MGGA local counterparts, for instance, BH-LYP vs B-LYP, PBE0 vs PBE, TPSSh vs TPSS or even B3-LYP

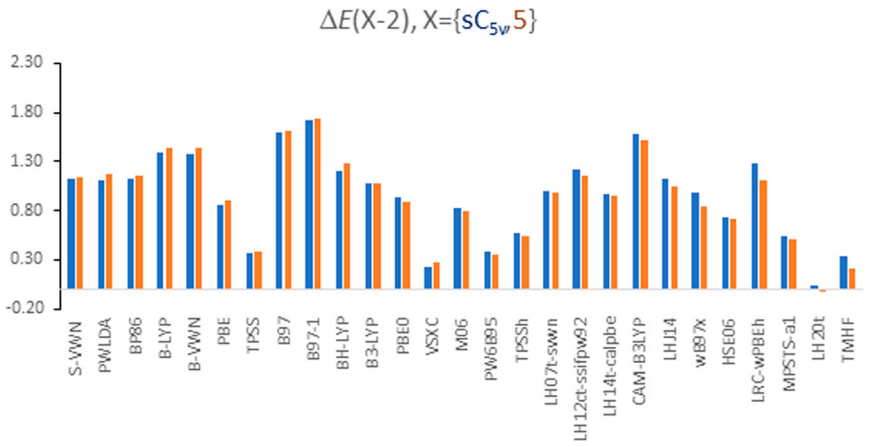

Figure 2. DFT comparison of the energy differences between isomers **5** and **2**, including structure $\mathbf{sC_{5v}}$ (a saddle point of C_{5v} symmetry very close geometrically to isomer **5**). The $\Delta E(\mathbf{X}-\mathbf{2})$ values ($\mathbf{X} = \mathbf{sC_{5v}}$,**5**), are given in eV and correspond to the lowest-lying electronic states of each structure by the corresponding density functional. The dhf-TZVP basis has been used and the computations are done on the TPSSh/dhf-TZVP optimised geometries.

vs BP86 or B-VWN, one observes no obvious correlation with the amount of exact exchange, the **5**−**2** energy differences being sometimes relatively similar. In other words, inclusion of exact exchange does not generally lead to smaller **5**−**2** energy differences. Comparing the range-separated hybrids with the parent or most similar hybrid GGA or MGGA density functional (Figure S1) one observes a clearly reduced energy difference in ωB97x as compared to B97, a much larger value in CAM-B3LYP as compared to B3-LYP. There is no clear correlation neither between the amount of spin contamination in the Kohn–Sham (KS) determinant of isomer **5** and the **5**−**2** energy difference (isomer **2** presents little spin contamination in its quartet state by most computations), although the density functionals which give low or negative (LH20t) **5**−**2** energy differences produce moderate spin contaminations for isomer **5** (see Figure S2). We have also tested some Minnesota density functionals, from M05 [89] to some of the non-separable ones, see Figure S3a. Most of those functionals give positive **5**−**2** energy differences, ranging from small in the case of the non-separable ones, to relatively large in the case of the revised versions of M06(-l) [90]. Remarkably MN12-l [91] gives a lower difference than the screened-exact-exchange MN12-sx [18]. Two functionals, M06-l [92] and M06-2x [80] (the latter was parametrised only for nonmetals, therefore not really adequate for the present case), give negative energy differences, even when M06 gives a sizeable positive value. It must be further noted that the revised version of TPSS (revTPSS) [93], its regularised version [94] (regTPSS) and the PBE functional for solids (PBEsol) [95], all give quite similar results for the **5**−**2** energy difference as their general-purpose counterparts (see Figure S3b).

The local hybrids TMHF and LH20t give small or negative **5**−**2** energy differences. They are both based on the meta-GGA B95 correlation functional, but while TMHF uses the Tao-Mo (TM) exchange [88] that of LH20t is based on the PBE functional. The adjustable parameters of LH20t have been obtained by using thermochemical and kinetic data, while TMHF has been defined from first principles (i.e. without using thermochemical test sets), still giving very good statistical performance. For instance, both functionals display similar deviations in the W4-11-atomisation-energies subset [96] of the GMTKN55 test set [97], LH20t giving a mean standard deviation (MSD) smaller in magnitude and TMHF giving a lower root-mean-square deviation, both outperforming TPSS, TPSSh, and TM, as well as other local-hybrid density functionals [16,17]. In the BH76 subset for reaction barrier heights [98–100], LH20t is slightly superior to TMHF, and both are significantly better than TPSSh or TM [16]. They also perform similarly well in a test of 41 excitation energies of small molecules, TMHF giving the smallest MSD value among the tested functionals. The long-range-corrected ωB97x-D density functional [19,101], which also includes an empirically determined dispersion correction, provides MSD values lying within those of TMHF and LH20t (BH76), or a little higher in magnitude (W4-11) [16]. It must be noted that TMHF and LH20t differ in the form of the local mixing function (LMF), also in the fact that the latter is constructed with a calibration function of the pig2 (partial integration gauge 2) type, which is based on the B88 exchange functional [72]. While LH20t uses a LMF based on the iso-orbital indicator (t-LMF) [2], TMHF uses a more complex one based on the correlation length proposed by Johnson [14], used in the argument of an exponential

term, such that the LMF tends to 1 at long distances [16]. The latter tends to be relatively small at the position of the nuclei while the former can take relatively high values there, still being small along the bonds [15]. It must also be noted that in LH20t, B95 is re-parametrised, and also that the PBE GGA correction to the LSDA exchange enters with a factor of 0.781. It must also be recalled that ωB97x has a small fraction of short-range exact exchange in addition to the long-range correction part [19]. Finally, it is remarkable that LH20t has been found to give a very good performance in the MVO-10 set (mixed-valence, metal–oxide systems), where it describes equally well localised and highly delocalised systems, in contrast to the other functionals tested, even when ωB97x-D also gives a good average performance [15]. None of these functionals eliminates self-interaction completely. LH20t has been tried in the SIE4x4 test [97], which consists of dissociation-energy calculations for symmetric dimer cations of first-row atoms and simple molecules done at several interatomic distances with moderately good results [15].

It must be noted that the MPSTS functional [13] also has a very sophisticated LMF, but does not perform as well as LH20t or TMHF [16].

Using TM exchange [88] together with B95 correlation [87], without exact exchange, what we call here TMB95, one gets a very sizeable negative **5−2** energy difference, −0.35 eV. Thus, in this case, the effect of including exact exchange in the form of a local hybrid (TMHF) is not really small. PBEB95, that is the PBE exchange [74] and B95 [87] correlation functionals put together, gives a small but positive difference of 0.14 eV. Going back to the density-functional comparison with the full set of functionals, one can observe a sort of convergence: the most sophisticated functionals tend to give small **5−2** energy differences, but there is not a real correspondence between performance and the rung of 'Jacob's ladder'. TMHF and LH20t have a good combination of correlation and exchange parts, include reasonable LMFs and, LH20t, has a calibration function, determined such that the weight of the GGA part of the exchange is diminished in comparison with the original PBE density functional. Although the test sets in which both are tried do not include metal clusters, they both provide very good performance in all of them, which is indicative that both should be tried in metal clusters as well. Since they are constructed very differently, TMHF is derived from first principles (i.e. without using thermochemical test sets), they can be used to somehow bracket the exact result.

Therefore, we have also used LH20t for the 2c and X2C computations. By the 2c-LH20t/dhf-TZVPPD-2c method, one gets 0.04 eV while at the X2C-LH20t/x2c-TZVPall-2c level, the **5−2** energy difference is −0.35 eV (that of TMHF is −0.18 eV).

We have also checked the density-functional dependence of the RPA **5−2** energy difference, calculated by the dRPA method and occasionally by the ACSOSEX and AXK beyond-RPA methods. Only a subset of the density functionals considered in the former DFT comparisons have been used. Kohn–Sham orbitals produced by semi-local density functionals, should, in principle, be preferred [6,7], and TPSS has often been used. But the TPSSh KS spin-orbitals and energies produce quite similar values [7], also here. We have used the TPSS, TM, TMB95, PBE, BP86, B-LYP and B-VWN density functionals, but also tested the related hybrid density functionals TPSSh, TMHF, LH20t, PBE0, B3-LYP, BH-LYP, B97, and ωB97x. The results are given in Table S3 of the SD (see also the addendum for basis set dependence), also Figures S4a to S4c. The **5−2** energy differences obtained by dRPA can be grouped in three sets, quite independently of the DFT energy difference: TPSS, TM, and TMB95 give values from 0.37 to 0.46 eV while PBE, B-LYP, BP86 and B-VWN give values in the range 0.62–0.67 eV. The hybrid density functionals give somewhat less deep dRPA energies than their semi-local counterparts, but the **5−2** dRPA energy differences are usually very similar. TPSSh gives 0.36 eV, PBE0 0.54, B3-LYP 0.66, B97 0.63 eV while LH20t gives 0.35 eV. TMHF, BH-LYP, and ωB97x, however, give even less deep dRPA energies and very high **5−2** energy differences. Note (Figures S4a to S4c) that hybrid functionals produce larger HOMO–LUMO gaps, give somewhat deeper KS expectation values of the Hamiltonian, but less deep correlation energies, such that the total dRPA energies are also less deep. The latter may tend to correlate with larger **5−2** energy differences, but that is only apparent in the case of the most extreme functionals by that measure, namely BH-LYP, TMHF and ωB97x.

It must be noted that the AXK method performs well in several subsets of the GMTKN55 test set [5], for instance the BHDIV10 subset for reaction barrier heights [97], and the ADIM6 subset for the noncovalent n-alkane dimers [102]. Its performance with the SIE4x4 test set is better than that of dRPA, giving, interestingly, positive errors while ACSOSEX gives negative ones, typically of the same magnitude, even for long inter-fragment distances [5]. In the 3d-transition-metal training set defined by Furche and Perdew [103] though, it produces significant errors in the dissociation energies, not being better on average than dRPA and only improving on ACSOSEX, the worse performance being that obtained in the dissociation energies of the Sc, V and Ni dimers, where

Table 4. Beyond-RPA and 2c-RPA DFT comparison. The dhf-TZVPPD-2c basis set has been used. ΔE values are given in eV. The DFT and dRPA energy differences are given for comparison, also the values computed with the dhf-QZVPPD-2c basis set.

	$\Delta E_{\mathrm{DFT}}(\mathbf{5}-\mathbf{2})^{(a)}$		$\Delta E_{\mathrm{dRPA}}(\mathbf{5}-\mathbf{2})^{(a)}$		$\Delta E_{\mathrm{AXK}}(\mathbf{5}-\mathbf{2})^{(a)}$		$\Delta E_{\mathrm{ACSOSEX}}(\mathbf{5}-\mathbf{2})$	$\Delta E_{\mathrm{2c-DFT}}(\mathbf{5}-\mathbf{2})$	$\Delta E_{\mathrm{2c-RPA}}(\mathbf{5}-\mathbf{2})$
TPSS	0.42	0.41	0.37	0.28	0.62	0.55	0.90	0.45	0.34
TPSSh	0.60	0.58	0.36	0.28	0.71	0.67	1.05	0.62	0.40
TMHF	0.32	0.29	1.18	1.08	1.22	1.17	1.15	0.12	1.20

(a) dhf-QZVPPD-2c results on the rightmost column.

the (DFT) TPSS or TPSS-D3 calculations alone give much better results than dRPA, AXK, ACSOSEX, and largely than ACSOX (the bare second-order exchange kernel method), that being the ordering for decreasing performance. In all those tests, the def2-QZVPP basis set [104] was used, the results being very similar to the complete-basis-set limits when calculated by the correlation-consistent aug-cc-pVXZ basis set series (X = T,Q,5) [105–107]. It must also be noted that the AXK@TPSS(h) energies in the complete-basis-set limit are very close to the exact non-relativistic energies for the atoms H-Ne [7]. AXK performs quite well in the non-relativistic atomisation energies of the HEAT test [108], as well as in the properties of transition-metal monoxides, although other beyond-RPA, Bethe-Salpeter-based methods, have been found to provide better performance in those tests, clearly improving on the corresponding (DFT) TPSS(h) calculations [7].

Table 4 presents a DFT and RPA comparison between the TPSS and TPSSh density functionals, to which we have added TMHF. By the ACSOSEX method the TPSS, TPSSh and TMHF KS spin-orbitals and energies produce similar results, close to 1 eV. By the AXK method, the TPSS and TPSSh energy differences go to 0.62 eV-0.71 eV while TMHF stays above 1 eV. The AXK and ACSOSEX correlation energies are significantly less deep than their dRPA counterparts, by about 1.7 E_{h} (AXK) or 2.2 E_{h} (ACSOSEX) with the TPSS density functional, the corrections being a little bit smaller, by about 0.1 E_{h}, with TPSSh. By the 2c-RPA@TPSSh computation, the **5**−**2** energy difference is 0.40 eV, almost the same as with (1c) dRPA, and significantly lower than the 2c-TPSSh value of 0.62 eV. The corresponding TPSS results are very similar. With the dhf-QZVPPD-2c basis set, the dRPA energy differences are reduced by about 0.1 eV as compared to their dhf-TZVPPD-2c counterparts, so similar reductions in the 2c-RPA results can be expected.

As said, the AXK and even more the ACSOSEX corrections to the dRPA correlation energies are relatively large, but still far from those of SOX. The average coupling strength $\bar{\alpha}$, defined as the difference between the SOX and AXK corrections relative to the SOX correction can be used as a test of the accuracy of the AXK method. With values larger than 0.5 the AXK energies may be affected by large errors, although there could be some exceptions [5]. Considering the two isomers, **5** and **2**, we have $\bar{\alpha}(5) = 0.50(0.48)$ and $\bar{\alpha}(2) = 0.49(0.46)$, for the AXK@TPSS(h) methods, which suggests that AXK is likely not an improvement over dRPA or even (DFT) TPSS(h). According to the results on the benchmark tests, ACSOSEX could even be less so. It must also be noted that ACSOSEX is one-electron self-correlation free and gives half the correlation energy of dRPA in two-electron singlets [5,6,109]. Indeed, ACSOSEX@TPSS(h) increasingly underestimates the non-relativistic energies from He, by 1 (2) mE_{h}, to Ne, by 23 (27) mE_{h}, while AXK@TPSS(h) stays quite close to the exact value, slightly overshooting for larger non-dynamical correlation (the largest differences being −11 mE_{h} in Be (−7 mE_{h} in Li) for AXK@TPSS(h)) [7].

Therefore, we tend to attach more relevance to DFT, 2c-DFT, and the corresponding dRPA results in what concerns the energetics of the Ta_{12}^- isomers.

In conclusion, 2c-DFT computations by the TMHF and LH20t density functionals (see above) give very small values for the **5**−**2** energy difference. The corresponding dRPA@TPSSh and 2c-RPA@TPSSh values are positive but quite small values. The all-electron X2C/x2c-TZVPall-2c computations give negative energy differences with both TMHF and LH20t. Considering together those results we conclude that the **5**−**2** energy difference could indeed be very small, perhaps even negative.

It also must be noted that taking into account temperature and entropic effects by chemical potential calculations (T = 95 K) does not change the relative energies too much [1], the **5**−**2** energy difference would be reduced by less than 0.1 eV at 95 K (TPSSh/dhf-TZVP geometries and vibrational frequencies). Inclusion of dispersion corrections by the D3-BJ and D4 methods [110–112] increase the **5**−**2** energy difference very little, both by about 0.03 eV. If the exact **5**−**2** energy difference were very small but still positive and considering the PBP-based isomers **3** to **5** together, that is, assuming small activation barriers, increasing the temperature would favour the stability of the **3**–**5** manifold. Therefore, in thermal equilibrium, there could be a temperature range where there is a mixture of isomers.

Since isomer **2** is not consistent with the scattering profile found in the TIED experiments, we have explored the possibility of kinetic trapping. For that

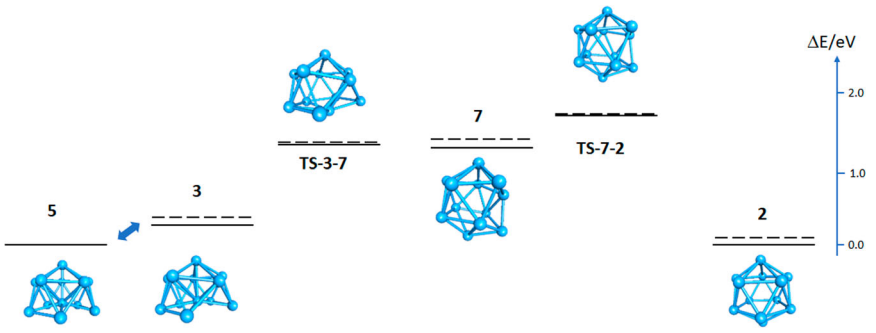

Figure 3. Reaction coordinate calculated by the TPSSh/def2-SVP method for the lowest quartet and doublet states, and relative energies (eV) calculated by the 2c-TMHF/dhf-TZVP-2c method on the geometries reoptimized at the TPSSh/dhf-TZVP level. Isomer **7** is an intermediate [1]. Broken lines correspond to energies computed using the optimised geometries of the doublet state.

purpose, we have located the reaction coordinate connecting isomers **3** and **2** by TPSSh/def2-SVP computations [113] and reoptimized the stationary points by the TPSSh/dhf-TZVP method. We have then done 2c-TMHF/dhf-TZVP-2c computations on those optimised geometries. The relative energies corresponding to the saddle points of the **3**↔**5** conversion are close to that of **5** at the optimisation level, so we conclude that such a process has a small barrier, which cannot be accurately determined without further geometry re-optimizations. The results are shown in Figure 3 and clearly suggest a relatively large energy barrier for the **5**↔**2** conversion, beyond 1 eV and larger for the reverse process. It is not completely a consequence of the choice of the density functional. By 2c-BH-LYP/dhf-TZVP-2c computations on the TPSSh/def2-SVP geometries, isomer **3** lies well above **2**, by about 1 eV, likely too large a difference, but there is still a barrier of about 0.5 eV for the **3**→**2** conversion. By the TPSSh/dhf-TZVP method **3** lies above **2** by 0.39 eV and the **3**→**2** barrier is 0.7 eV, about the same as with the 2c-TPSSh/dhf-TZVP-2c method. Note that isomerisation entails a very significant rearrangement of the cluster atoms, so small values for the **3**−**2** or **5**−**2** energy differences may come with high **3**→**2** isomerisation barriers. Note also that structures **3**–**5** are less compact than **2**, which may also favour kinetic trapping.

Furthermore, it must be noted that Ta_{11}^- has been found to have a PBP-based structure (incomplete icosahedron), similar to isomers **2**–**5** with one atom less around one PBP tip [1]. Also, that by adding one atom to isomer **5** one easily gets an icosahedral Ta_{13}^- isomer. In fact, from Ta_9^- to Ta_{12}^- the TIED experiments point to PBP-based/incomplete icosahedral structures [1].

From the computations above, we conclude that isomer **5**, isomers **3** to **5** in general, are very close in energy to **2**, but also that the **5**↔**2** isomerisation is prevented by, at least, a moderate, more likely high energy barrier. It must be added that isomer **1**, which has an HBP-based structure, is, by the TPSSh density functional, also very close to isomers **2** and **5**, see Table S4. The barrier for the **5**→**1** isomerisation is about 0.8–0.9 eV by 2c-TPSSh computations, see Figure S5 for details.

Given there is experimental information on neutral and cationic Ta clusters, it is interesting to take into account isomers **5** and **2** of the neutral and cationic system and compare them with the negatively charged system ($Ta_{12}^{(-,0,+)}$). The results are given in the SD, Tables S5 and S6. Ta_{12} has been found to have nearly zero magnetic moment in the low-*T* deflection experiments of Díaz-Bachs *et al.* [31], to have two threshold-ionisation energies in the experiments of Collings *et al.*, probably arising from the existence of two different isomers [33], and the kinetic experiments of Hamrick and Morse [32] are also consistent with the existence of two isomers. The IR-MPD experiments of Gruene *et al.* [30] on the cationic Ta clusters show only few and weak peaks in the case of Ta_{12}^+, so no indication can be made on the existence of two isomers. The DFT computations of Du *et al.* [53] give the best agreement with the IR-MPD experiments for a five-capped PBP isomer of Ta_{12}^+, similar to isomers **3** to **5**, which they find to be very high lying, the icosahedral isomer, similar to **2**, being the lowest lying. The DFT computations of Li *et al.* [52] on the neutral systems also point to the icosahedral motif as the lowest-lying form of Ta_{12}, the five-capped PBP and the four-capped HBP being much higher in energy. It must also be noted that the results of our isomer search for Ta_{12}^- by a genetic algorithm [1] are very much in line with the recent ones on the neutral clusters obtained by Han *et al.* by deep-neural-network techniques [55]. Generally speaking, the comparison between DFT and experimental results points to the need of better functionals.

Table S5 presents the **5**−**2** energy differences for $Ta_{12}^{(-,0,+)}$ computed by the 2c-TMHF method with both the dhf-TZVP-2c and the dhf-TZVPPD-2c basis sets,

Table 5. Energy differences **2**−**1** between two competing isomers of Ta_{10}^- (**1**, bicapped square antiprism and **2**, tricapped pentagonal bipyramid) calculated by the TPSSh, TMHF and LH20t density functionals. ΔE_{DFT}(**2**−**1**) and ΔE_{2c-DFT}(**2**−**1**) represent the one and 2c energy differences calculated with the pseudopotential, $\Delta E_{X2C-DFT}$(**2**−**1**) is the energy difference computed by the X2C method with the all-electron basis sets. ΔE_{2c-RPA}(**2**−**1**) is the 2c-RPA energy difference. The dhf-TZVPPD-2c (TZ) and dhf-QZVPPD-2c (QZ) as well as the all-electron x2c-TZVPall-2c (x2c-TZ) and x2c-TZVPPall-2c (x2c-TZP) basis sets have been used.

	ΔE_{DFT}(**2**−**1**)[(a)]	ΔE_{2c-DFT}(**2**−**1**)[(b)]		ΔE_{2c-RPA}(**2**−**1**)		$\Delta E_{X2C-DFT}$(**2**−**1**)[(b)]	
	TZ	TZ	QZ	TZ	QZ	x2c-TZ	x2c-TZP
TPSSh	0.21	0.14	0.13	0.15	0.15	0.16	0.12
TMHF	−0.13	−0.29	−0.30	0.42	0.41	−0.31	−0.31
LH20t	0.20	0.12	0.10	0.13	0.13	0.08	0.06

(a) Isomer **1** is in a $^2B_1$ (D_{4d}) state and isomer **2** in a $^4A_2$ (C_{3v}) state. The 2c computations have been done in C_1 symmetry.
(b) Average numbers of unpaired electrons N_s for isomers **1** and **2**. 2c-TPSSh: N_s(**1**) = 0.96, N_s(**2**) = *2.94*; 2c-TMHF: N_s(**1**) = 0.91, N_s(**2**) = 0.14; 2c-LH20t: N_s(**1**) = 0.95, N_s(**2**) = 2.76 with the dhf-TZVPPD-2c basis set and N_s(**1**) = 0.96, N_s(**2**) = *2.96*; 2c-TMHF: N_s(**1**) = 0.91, N_s(**2**) = 0.79; 2c-LH20t: N_s(**1**) = 0.95, N_s(2) = 2.91 with the dhf-QZVPPD-2c basis set. X2C-TPSSh: N_s(**1**) = 0.93, N_s(**2**) = 2.93; X2C-TMHF: N_s(**1**) = 0.88, N_s(**2**) = 1.11; X2C-LH20t: N_s(**1**) = 0.92, N_s(**2**) = 2.88 with the x2c-TZVPall-2c basis set. X2C-TPSSh: N_s(**1**) = 0.93, N_s(**2**) = 2.95; X2C-TMHF: N_s(**1**) = 0.87, N_s(**2**) = 1.97; X2C-LH20t: N_s(**1**) = 0.92, N_s(**2**) = 2.90 with the x2c-TZVPPall-2c basis set.

together with the average number of unpaired electrons N_s, resulting in each of the computations. It is readily seen that the **5**−**2** energy differences are all positive but quite small, the largest value is that of the neutral system, 0.43 eV, that of the cation is about 0.3 eV. We have also done 2c-RPA computations using the TPSSh density functional (Table S6). The **5**−**2** energy difference computed by the 2c-TPSSh/dhf-TZVPPD-2c method for the neutral system is positive, about the same as in Ta_{12}^-. Interestingly, for the neutral system, the corresponding 2c-RPA@TPSSh computations point to isomer **5** having nearly-zero average number of unpaired electrons, the Kramers-restricted and unrestricted computations giving almost coincident energies. For isomer **2**, we have obtained two neatly different self-consistent-field (SCF) solutions, one with N_s = 1.63, the other Kramers-restricted, being almost isoenergetic by 2c-RPA. That result is also in agreement with the low-T magnetic deflection experiments on the neutral clusters [31], so it is not really helpful to determine which Ta_{12} isomer is present in them.

We have also taken on the case of Ta_{10}^-, where there is an isomer competition between isomer **2**, a tricapped PBP, and isomer **1**, a bicapped square antiprism (Figure 4), the latter appearing as a little more stable by previous computations, but poorly fitting to the TIED scattering profile, while **2** is the good-fitting one [1]. Huang *et al.* [56] find in their PES experiments isomer **1** to be the one responsible for some bands of the Ta_{10}^- photoelectron spectrum.

We have done a few DFT, 2c-DFT, and the corresponding 2c-RPA computations as well as X2C-DFT computations, using the TPSSh, TMHF, and LH20t density functionals. The results are presented in Table 5. In the 2c computations, the TMHF density functional predicts **2** to lie below **1** by about −0.30 eV, while TPSSh and LH20t give small positive energy differences, just 0.06 eV in the X2C-LH20t/dhf-TZVPPall-2c computation. In the

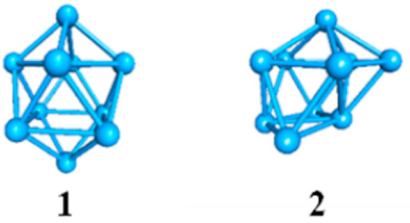

Figure 4. The two isomers of Ta_{10}^- considered in the present work.

series of DFT calculations, from 1c-DFT with the dhf-TZVPPD-2c basis set to X2C with x2c-TZVPPall-2c, the **2**−**1** energy difference diminishes with the three density functionals, by 0.09 eV (TPSSh), 0.14 eV (LH20t) and 0.18 eV (TMHF). Note that here, it is the TMHF density functional rather than LH20t the one that favours the PBP motif (although the PBP is quite open in one tip). Entropic effects may slightly favour isomer **2**, by less than 0.1 eV [1] at 95 K. There could also be a significant barrier to isomerisation, about 1.5 eV (**1**→**2**) by the 2c-TPSSh/dhf-TZVPPD-2c method, applied to TPSSh/dhf-TZVP optimised geometries (see Figure S6 and accompanying data).

We have also studied the density-functional dependence of the **2**−**1** energy difference, by using subsets of the functionals employed for Ta_{12}^- in DFT and dRPA computations. The results are presented in the SD, see Figure S7. There is also considerable dispersion on the DFT values, but not as much as in the case of Ta_{12}^-. TMHF gives a slightly negative value, ωB97x and BH-LYP give very small positive values, while those of TPSSh and LH20t are 0.21 and 0.20 eV, respectively (see also Table 5). The dRPA energy differences (1c) are all very small but positive, most of the density functionals giving values close to 0.2 eV. Note that in Ta_{10}^- most density functionals give only moderately small spin contaminations. Concerning the 2c-RPA **2**−**1** energy differences,

we attach more importance to those obtained with the TPSSh and LH20t functionals, for the 2c-RPA@TMHF absolute energies are probably not deep enough.

4. Conclusions

We have studied the competing isomers of Ta_{12}^- with recently developed density functionals and RPA methods, including two-component DFT and RPA methods. Our results suggest that very sophisticated density functionals, even more sophisticated than the local hybrids TMHF and LH20t, are needed to determine reliable energy differences between different motifs in Ta_n^- clusters by DFT and 2c-DFT methods. That is likely to happen in other TM clusters too. Those 2c-DFT computations should include all-electron basis sets as much as possible. We have tested here the exact two-component approach X2C including spin–orbit coupling. MGGA density functionals like TPSS and TPSSh in combination with RPA-type methods, including 2c-RPA, both Kramers-restricted, where applicable, and unrestricted, could be sufficient to establish the energy ordering between different SCF solutions in the same isomer or even between different isomers having the same motif. Combining those results with the experimental information on magnetic moments for instance, may help to determine which isomer is present in those experiments, and should also be taken into account in the assessment of the energy differences.

With such an approach, we obtain results for anionic, neutral and cationic Ta_{12}, and also for Ta_{10}^-, which are moderately consistent with the experiments.

In the particular case of Ta_{12}^-, the reaction coordinate for the conversion of the isomer with a PBP motif to the icosahedral cage presents a relatively high-lying saddle point, which may hinder isomerisation, especially if the energy difference between those two isomers is small, as the local-hybrid-DFT and dRPA@TPSS(h) one and two-component calculations suggest. Another isomer, based on the HBP motif, is also very close in energy, the isomerisation barrier to the isomers with the PBP motif being about 1 eV.

Acknowledgements

We thank Laurenz Monzel (Saarland University) and Christof Holzer (Karlsruhe Institute of Technology) for help with details of the computations with Turbomole. Our research was supported by the Bundesministerium für Bildung und Forschung (BMBF) through the Helmholtz Association via the PoF IV programme 'Materials Systems Engineering' (MSE). JRF acknowledges support from the Xunta de Galicia by the GRC programme. D.S. is thankful for financial support by the German Research Foundation (Deutsche Forschungsgemeinschaft, DFG) through project SFB 1441 – Project-ID 426888090.

Disclosure statement

No potential conflict of interest was reported by the author(s).

Funding

This work was supported by Bundesministerium für Bildung und Forschung (BMBF): PoF IV program "Materials Systems Engineering"; Xunta de Galicia: GRC Program; German Research Foundation (Deutsche Forschungsgemeinschaft, DFG): project SFB 1441 – Project-ID 426888090.

References

[1] M. Kraft, J.R. Flores, W. Klopper, M.M. Kappes and D. Schooss, J. Phys. Chem. A. **125**, 3135–3145 (2021). doi:10.1021/acs.jpca.1c01250

[2] J. Jaramillo, G.E. Scuseria and M. Ernzerhof, J. Chem. Phys. **118**, 1068–1073 (2003). doi:10.1063/1.1528936

[3] C. Holzer, Y.J. Franzke and M. Kehry, J. Chem. Theory Comput. **17**, 2928–2947 (2021). doi:10.1021/acs.jctc.1c00203

[4] H. Eshuis, J.E. Bates and F. Furche, Theor. Chem. Acc. **131**, 1084 (2012). doi:10.1007/s00214-011-1084-8

[5] G.P. Chen, M.M. Agee and F. Furche, J. Chem. Theory Comput. **14**, 5701–5714 (2018). doi:10.1021/acs.jctc.8b00777

[6] J.E. Bates and F. Furche, J. Chem. Phys. **139**, 171103 (2013). doi:10.1063/1.4827254

[7] C. Holzer, X. Gui, M.E. Harding, G. Kresse, T. Helgaker and W. Klopper, J. Chem. Phys. **149**, 144106 (2018). doi:10.1063/1.5047030

[8] K. Krause and W. Klopper, J. Chem. Phys. **139**, 191102 (2013). doi:10.1063/1.4832738

[9] M. Kühn, J. Chem. Theory Comput. **10**, 623–633 (2014). doi:10.1021/ct400994x

[10] C. Holzer, J. Chem. Theory Comput. **19**, 3131–3145 (2023). doi:10.1021/acs.jctc.3c00156

[11] M.K. Armbruster, F. Weigend, C. van Wüllen and W. Klopper, Phys. Chem. Chem. Phys. **10**, 1748–1756 (2008). doi:10.1039/B717719D

[12] D. Peng, N. Middendorf, F. Weigend and M. Reiher, J. Chem. Phys. **138**, 184105 (2013). doi:10.1063/1.4803693

[13] J.P. Perdew, V.N. Staroverov, J. Tao and G.E. Scuseria, Phys. Rev. A. **78**, 052513 (2008). doi:10.1103/PhysRevA.78.052513

[14] E.R. Johnson, J. Chem. Phys. **141**, 124120 (2014). doi:10.1063/1.4896302

[15] M. Haasler, T.M. Maier, R. Grotjahn, S. Gückel, A.V. Arbuznikov and M. Kaupp, J. Chem. Theory Comput. **16**, 5645–5657 (2020). doi:10.1021/acs.jctc.0c00498

[16] C. Holzer and Y.J. Franzke, J. Chem. Phys. **157**, 034108 (2022). doi:10.1063/5.0100439

[17] A.V. Krukau, O.A. Vydrov, A.F. Izmaylov and G.E. Scuseria, J. Chem. Phys. **125**, 224106 (2006). doi:10.1063/1.2404663

[18] R. Peverati and D.G. Truhlar, Phys. Chem. Chem. Phys. **14**, 16187–16191 (2012). doi:10.1039/c2cp42576a

[19] J.-D. Chai and M. Head-Gordon, J. Chem. Phys. **128**, 084106 (2008). doi:10.1063/1.2834918

[20] A. Fielicke, Chem. Soc. Rev. **52**, 3778–3841 (2023). doi:10.1039/D2CS00104G

[21] W.A. de Heer, Rev. Mod. Phys. **65**, 611–675 (1993). doi:10.1103/RevModPhys.65.611

[22] D. Schooss and M.M. Kappes, in *Encyclopedia of Interfacial Chemistry*, edited by K. Wandelt (Elsevier, Oxford, 2018). pp. 567–579. doi:10.1016/B978-0-12-409547-2.12963-4

[23] D. Schooss, M.N. Blom, J.H. Parks, B.V. Issendorff, H. Haberland and M.M. Kappes, Nano Lett. **5**, 1972–1977 (2005). doi:10.1021/nl0513434

[24] E. Waldt, A.-S. Hehn, R. Ahlrichs, M.M. Kappes and D. Schooss, J. Chem. Phys. **142**, 024139 (2015). doi:10.1063/1.4905267

[25] R. Moro, X. Xu, S. Yin and W.A. de Heer, Science. **300**, 1265–1269 (2003). doi:10.1126/science.1083247

[26] M.B. Knickelbein, J. Chem. Phys. **116**, 9703–9711 (2002). doi:10.1063/1.1477175

[27] X. Xu, S. Yin, R. Moro, A. Liang, J. Bowlan and W.A. de Heer, Phys. Rev. Lett. **107**, 057203 (2011). doi:10.1103/PhysRevLett.107.057203

[28] F. Rivic, T.M. Fuchs and R. Schäfer, Phys. Chem. Chem. Phys. **23**, 9971–9979 (2012). doi:10.1039/d1cp00351h

[29] J. Meyer, M. Tombers, C. van Wüllen, G. Niedner-Schatteburg, S. Peredevkov, W. Eberhardt, M. Neeb, S. Palutke, M. Martins and W. Wurth, J. Chem. Phys. **143**, 104302 (2015). doi:10.1063/1.4929482

[30] P. Gruene, A. Fielicke and G. Meijer, J. Chem. Phys. **127**, 234307 (2007). doi:10.1063/1.2806177

[31] A. Diaz-Bachs, M.I. Katsnelson and A. Kirilyuk, New J. Phys. **20**, 043042 (2018). doi:10.1088/1367-2630/aab5ca

[32] Y.M. Hamrick and M.D. Morse, J. Phys. Chem. **93**, 6494–6501 (1989). doi:10.1021/j100354a042

[33] B.A. Collings, D.M. Rayner and P.A. Hackett, Int. J. Mass Spectrom. Ion Proc. **125**, 207–214 (1993). doi:10.1016/0168-1176(93)80043-E

[34] M. Sakurai, K. Watanabe, K. Sumiyama and K. Suzuki, J. Chem. Phys. **111**, 235–238 (1999). doi:10.1063/1.479268

[35] D.E. Blumling, S.G. Sayres, M.W. Ross and A.W. Castleman, Jr., Int. J. Mass Spectrom. **333**, 55–58 (2013). doi:10.1016/j.ijms.2012.08.036

[36] L. Fang, X. Shen, X. Chen and J.R. Lombardi, J. Chem. Phys. **113**, 7178–7181 (2000). doi:10.1063/1.1312283

[37] B. Wang, H.-J. Zhai, X. Huang and L.-S. Wang, J. Phys. Chem. A. **112**, 10962–10967 (2008). doi:10.1021/jp806166h

[38] S.-G. He, Y. Xie, F. Dong and E.R. Bernstein, J. Chem. Phys. **125**, 164306 (2006). doi:10.1063/1.2360278

[39] G. Zwaschka, M. Rondelli, M. Krause, M.D. Rötzer, M.N. Hedhili, U. Heiz, J.-M. Basset, F.F. Schweinberger and V. D'Elia, New J. Chem. **42**, 3035–3041 (2018). doi:10.1039/c7nj04275b

[40] T. Masubuchi, J.F. Eckhard, G. Goddard, M. Tschurl and U. Heiz, Phys. Chem. Chem. Phys. **21**, 20743–20749 (2019). doi:10.1039/c9cp02739d

[41] J.F. Eckhard, T. Masubuchi, M. Tschurl, R.N. Barnett, U. Landman and U. Heiz, J. Phys. Chem. C. **122**, 25628–25637 (2018). doi:10.1021/acs.jpcc.8b07729

[42] K.A. Zemski, R.C. Bell and A.W. Castleman, J. Chem. Phys. A. **104**, 5732–5741 (2000). doi:10.1021/jp000051i

[43] K. Lange, B. Visser, D. Neuwirth, J.F. Eckhard, U. Boesl, M. Tschurl, K.H. Bowen and U. Heiz, Int. J. Mass Spectrom. **375**, 9–13 (2015). doi:10.1016/j.ijms.2014.10.010

[44] D. Neuwirth, J.F. Eckhard, B.R. Visser, M. Tschurl and U. Heiz, Phys. Chem. Chem. Phys. **18**, 8115–8119 (2016). doi:10.1039/c5cp07245j

[45] M. Arakawa, K. Ando, S. Fujimoto, S. Mishra, G.N. Patwari and A. Terasaki, Phys. Chem. Chem. Phys. **20**, 13974–13982 (2018). doi:10.1039/c8cp00424b

[46] C. Geng, J. Li, T. Weiske and H. Schwarz, Proc. Natl. Acad. Sci. U.S.A. **115**, 11680–11687 (2018). doi:10.1073/pnas.1814610115

[47] N. Levin, J. Lengyel, J.F. Eckhard, M. Tschurl and U. Heiz, J. Am. Chem. Soc. **142**, 5862–5869 (2020). doi:10.1021/jacs.0c01306

[48] A. Jiang, T.A. Tyson and L. Axe, J. Phys. Condens. Matter. **17**, 6111–6121 (2005). doi:10.1088/0953-8984/17/39/001

[49] W. Fa, C. Luo and J. Dong, J. Chem. Phys. **125**, 114305 (2006). doi:10.1063/1.2338890

[50] V. Kumar, Comput. Theor. Chem. **1021**, 149–154 (2013). doi:10.1016/j.comptc.2013.07.003

[51] M. Zhang and R. Fournier, Phys. Rev. A. **79**, 043203 (2009). doi:10.1103/PhysRevA.79.043203

[52] X. Li, Y. Chen, P. Basnet, J. Luo and H. Wang, RSC Adv. **9**, 1015–1028 (2019). doi:10.1039/c8ra09240k

[53] J. Du, X. Sun and G. Jiang, J. Chem. Phys. **136**, 094311 (2012). doi:10.1063/1.3690455

[54] J. Du, X. Sun, J. Chen, L. Zhang and G. Jiang, Dalton Trans. **43**, 5574–5579 (2014). doi:10.1039/c3dt53097c

[55] L. Han, G.-D. Jiang, X.-N. Li and S.-G. He, Chem. Phys. Lett. **785**, 139118 (2021). doi:10.1016/j.cplett.2021.139118

[56] B. Huang, H. Zhang, L. Geng and Z. Luo, J. Phys. Chem. Lett. **13**, 9711–9717 (2022). doi:10.1021/acs.jpclett.2c02410

[57] V.N. Staroverov, G.E. Scuseria, J. Tao and J.P. Perdew, J. Chem. Phys. **119**, 12129–12137 (2003). doi:10.1063/1.1626543

[58] A.D. Becke, J. Chem. Phys. **98**, 1372–1377 (1993). doi:10.1063/1.464304

[59] C. Lee, W. Yang and R.G. Parr, Phys. Rev. B. **37**, 785–789 (1988). doi:10.1103/PhysRevB.37.785

[60] J. Tao, J.P. Perdew, V.N. Staroverov and G.E. Scuseria, Phys. Rev. Lett. **91**, 146401 (2003). doi:10.1103/PhysRevLett.91.146401

[61] F. Weigend and A. Baldes, J. Chem. Phys. **133**, 174102 (2010). doi:10.1063/1.3495681

[62] D. Figgen, K.A. Peterson, M. Dolg and H. Stoll, J. Chem. Phys. **130**, 164108 (2009). doi:10.1063/1.3119665

[63] F. Weigend, Phys. Chem. Chem. Phys. **8**, 1057–1065 (2006). doi:10.1039/b515623h

[64] A. Hellweg and D. Rappoport, Phys. Chem. Chem. Phys. **17**, 1010–1017 (2015). doi:10.1039/c4cp04286g

[65] P. Pollak and F. Weigend, J. Chem. Theory Comput. **13**, 3696–3705 (2017). doi:10.1021/acs.jctc.7b00593

[66] P.A.M. Dirac, Proc. R. Soc. Lond. A. **123**, 714–733 (1929). doi:10.1098/rspa.1929.0094

[67] J.C. Slater, Phys. Rev. **81**, 385–390 (1951). doi:10.1103/PhysRev.81.385

[68] S.H. Vosko, L. Wilk and M. Nusair, Can. J. Phys. **58**, 1200–1211 (1980). doi:10.1139/p80-159

[69] Y.J. Franzke, R. Treß, T.M. Pazdera and F. Weigend, Phys. Chem. Chem. Phys. **21**, 16658–16664 (2019). doi:10.1039/C9CP02382H

[70] TURBOMOLE V7.x 20xx, a development of University of Karlsruhe and Forschungszentrum Karlsruhe GmbH, 1989–2007,: TURBOMOLE GmbH, since 2007; available from http://www.turbomole.com

[71] J.P. Perdew and Y. Wang, Phys. Rev. B. **45**, 13244–13249 (1992). doi:10.1103/PhysRevB.45.13244; Erratum doi:10.1103/PhysRevB.98.079904

[72] A.D. Becke, Phys. Rev. A. **38**, 3098–3100 (1988). doi:10.1103/PhysRevA.38.3098

[73] J.P. Perdew, Phys. Rev. B. **33**, 8822–8824 (1986). doi:10.1103/PhysRevB.33.8822 ; Erratum doi:10.1103/PhysRevB.34.7406

[74] J.P. Perdew, K. Burke and M. Ernzerhof, Phys. Rev. Lett. **77**, 3865–3868 (1996). doi:10.1103/PhysRevLett.77.3865; Erratum doi: 10.1103/PhysRevLett.78.1396

[75] A.D. Becke, J. Chem. Phys. **107**, 8554–8560 (1997). doi:10.1063/1.475007

[76] F.A. Hamprecht, A.J. Cohen, D.J. Tozer and N.C. Handy, J. Chem. Phys. **109**, 6264–6271 (1998). doi:10.1063/1.477267

[77] A.D. Becke, J. Chem. Phys. **98**, 5648–5652 (1993). doi:10.1063/1.464913

[78] M. Ernzerhof and G.E. Scuseria, J. Chem. Phys. **110**, 5029–5036 (1999). doi:10.1063/1.478401

[79] T. Van Voorhis and G.E. Scuseria, J. Chem. Phys. **109**, 400–410 (1998). doi:10.1063/1.476577

[80] Y. Zhao and D.G. Truhlar, Theor. Chem. Acc. **120**, 215–241 (2008). doi:10.1007/s00214-007-0310-x

[81] H. Bahmann, A. Rodenberg, A.V. Arbuznikov and M. Kaupp, J. Chem. Phys. **126**, 011103 (2007). doi:10.1063/1.2429058

[82] A.V. Arbuznikov and M. Kaupp, J. Chem. Phys. **136**, 014111 (2012). doi:10.1063/1.3672080

[83] A.V. Arbuznikov and M. Kaupp, J. Chem. Phys. **141**, 204101 (2014). doi:10.1063/1.4901238

[84] T.M. Maier, M. Haasler, A.V. Arbuznikov and M. Kaupp, Phys. Chem. Chem. Phys. **18**, 21133–21144 (2016). doi:10.1039/C6CP00990E

[85] T. Yanai, D.P. Tew and N.C. Handy, Chem. Phys. Lett. **393**, 51–57 (2004). doi:10.1016/j.cplett.2004.06.011

[86] O.A. Vydrov and G.E. Scuseria, J. Chem. Phys. **125**, 234109 (2006). doi:10.1063/1.2409292

[87] A.D. Becke, J. Chem. Phys. **104**, 1040–1046 (1996). doi:10.1063/1.470829

[88] J. Tao and Y. Mo, Phys. Rev. Lett. **117**, 073001 (2016). doi:10.1103/PhysRevLett.117.073001

[89] Y. Zhao, N.E. Schultz and D.G. Truhlar, J. Chem. Phys. **123**, 161103 (2005). doi:10.1063/1.2126975

[90] Y. Wang, P. Verma, X. Jin, D.G. Truhlar and X. He, Proc. Natl. Acad. Sci. U.S.A. **115**, 10257–10262 (2018). doi:10.1073/pnas.1810421115

[91] R. Peverati and D.G. Truhlar, Phys. Chem. Chem. Phys. **14**, 13171–13174 (2012). doi:10.1039/c2cp42025b

[92] Y. Zhao and D.G. Truhlar, J. Chem. Phys. **125**, 194101 (2006). doi:10.1063/1.2370993

[93] J.P. Perdew, A. Ruzsinszky, G.I. Csonka, L.A. Constantin and J. Sun, Phys. Rev. Lett. **103**, 026403 (2009). doi:10.1103/PhysRevLett.103.026403, Erratum doi: 10.1103/PhysRevLett.106.179902

[94] A. Ruzsinszky, J. Sun, B. Xiao and G.I. Csonka, J. Chem. Theory Comput. **8**, 2078–2087 (2012). doi:10.1021/ct300269u

[95] J.P. Perdew, A. Ruzsinszky, G.I. Csonka, O.A. Vydrov, G.E. Scuseria, L.A. Constantin, X. Zhou and K. Burke, Phys. Rev. Lett. **100**, 136406 (2008). doi:10.1103/PhysRevLett.100.136406; Erratum, doi:10.1103/PhysRevLett.102.039902

[96] A. Karton, S. Daon and J.M.L. Martin, Chem. Phys. Lett. **510**, 165–178 (2011). doi:10.1016/j.cplett.2011.05.007

[97] L. Goerigk, A. Hansen, C. Bauer, A. Ehrlrich, A. Najibi and S. Grimme, Phys. Chem. Chem. Phys. **19**, 32184–32215 (2017). doi:10.1039/c7cp04913g

[98] Y. Zhao, B.J. Lynch and D.G. Truhlar, Phys. Chem. Chem. Phys. **7**, 43–52 (2005). doi:10.1039/B416937A

[99] Y. Zhao, N. González-García and D.G. Truhlar, J. Phys. Chem. A. **109**, 2012–2018 (2005). doi:10.1021/jp045141s

[100] L. Goerigk and S. Grimme, J. Chem. Theory Comput. **6**, 107–126 (2010). doi:10.1021/ct900489g

[101] J.D. Chai and M. Head-Gordon, Phys. Chem. Chem. Phys. **10**, 6615–6620 (2008). doi:10.1039/B810189B

[102] S. Grimme, J. Antony, S. Ehrlich and H. Krieg, J. Chem. Phys. **132**, 154104 (2010). doi:10.1063/1.3382344

[103] F. Furche and J.P. Perdew, J. Chem. Phys. **124**, 044103 (2006). doi:10.1063/1.2162161

[104] F. Weigend and R. Ahlrichs, Phys. Chem. Chem. Phys. **7**, 3297–3305 (2005). doi:10.1039/B508541A

[105] T.H. Dunning, Jr., J. Chem. Phys. **90**, 1007–1023 (1989). doi:10.1063/1.456153

[106] D.E. Woon and T.H. Dunning, Jr., J. Chem. Phys. **98**, 1358–1371 (1993). doi:10.1063/1.464303

[107] N.B. Balabanov and K.A. Peterson, J. Chem. Phys. **123**, 064107 (2005). doi:10.1063/1.1998907

[108] M.E. Harding, J. Vázquez, B. Ruscic, A.K. Wilson, J. Gauss and J.F. Stanton, J. Chem. Phys. **128**, 114111 (2008). doi:10.1063/1.2835612

[109] T.M. Henderson and G.E. Scuseria, Mol. Phys. **108**, 2511–2517 (2010). doi:10.1080/00268976.2010.507227

[110] S. Grimme, S. Ehrlich and L. Goerigk, J. Comput. Chem. **32**, 1456–1465 (2011). doi:10.1002/jcc.21759

[111] E. Caldeweyher, C. Bannwarth and S. Grimme, J. Chem. Phys. **147**, 034112 (2017). doi:10.1063/1.4993215

[112] E. Caldeweyher, S. Ehlert, A. Hansen, H. Neugebauer, S. Spicher, C. Bannwarth and S. Grimme, J. Chem. Phys. **150**, 154122 (2019). doi:10.1063/1.5090222

[113] P. Plessow, J. Chem. Theory Comput. **9**, 1305–1310 (2013). doi:10.1021/ct300951j